Dynamical crossover between hyperdiffusion and subdiffusion of polymer-grafted nanoparticles in a polymer matrix

Taiki Hoshino,[1,2,*] Daiki Murakami,[1,2] Yoshihito Tanaka,[2] Masaki Takata,[2] Hiroshi Jinnai,[1,2,3] and Atsushi Takahara[1,2,3,†]

[1]*ERATO Takahara Soft Interfaces Project, Japan Science and Technology Agency, CE80, Kyushu University, 744 Motooka, Nishi-ku, Fukuoka 819-0395, Japan*
[2]*RIKEN SPring-8 Center, 1-1-1 Kouto, Sayo, Hyogo 679-5148, Japan*
[3]*International Institute for Carbon-Neutral Energy Research (WPI-I2CNER), Kyushu University, Fukuoka, Japan*

The dynamical behavior of polystyrene-grafted silica nanoparticles dispersed in an atactic polystyrene matrix was studied using x-ray photon correlation spectroscopy. The time-autocorrelation functions were subjected to fitting analyses based on continuous-time random walk models. The nanoparticles exhibited non-Brownian behavior, and as the temperature increased, the crossover from hyperdiffusion to subdiffusion occurred at $1.25T_g$, where T_g is the glass transition temperature of the matrix polystyrene. Hyperdiffusive behavior is caused by the dynamical heterogeneity of the polymer matrix associated with the glass transition. When the temperature was higher than $1.25T_g$, the interaction of the grafted polymers with the polymer matrix became relatively significant, and caused a dramatic change in the dynamical behavior of the nanoparticles.

I. INTRODUCTION

Nanoparticles (NPs) in a fluid are thermally agitated and their dynamical behavior is strongly influenced by the surrounding matrix. The NPs in a Newtonian fluid move in a Brownian manner when there are no interactions between NPs. The mean squared displacement (MSD) of the NPs increases linearly with time, $\langle x^2(t) \rangle \propto (t)$. However, if the surrounding matrix is non-Newtonian or there are interactions between NPs, the MSD follows another power law, $\langle x^2(t) \rangle \propto (t)^\alpha$, with $a \neq 1$. If $0 < a < 1$, the NP behavior is subdiffusive. Subdiffusive behavior is commonly observed in constrained systems, such as living cells [1,2], actin networks [3], and crowded polymer systems [4–6]. In contrast, if $a > 1$, the NP behavior is hyperdiffusive or superdiffusive. This behavior is observed in soft solids, such as colloidal gels [7,8] and glass-forming systems [9–11].

To elucidate the driving force of non-Brownian NP behavior, the crossover between Brownian and non-Brownian NP behaviors has been studied by altering the properties of the surrounding matrix. Caronna *et al*. [10] investigated the dynamic properties of silica NPs suspended in a supercooled glass-forming liquid (1,2-propanediol) by x-ray photon correlation spectroscopy (XPCS). They observed the crossover from Brownian to hyperdiffusive behavior at $1.26T_g$ as the temperature decreased, where T_g is the calorimetric glass transition temperature of the liquid. Guo *et al*. [11] investigated the motion of suspensions of gold NPs in low-molecular-weight polystyrene (PS) with a plasticizer (toluene) by XPCS, in which the crossover from Brownian to hyperdiffusive behavior was observed at $1.1T_g$ as the temperature decreased. Sprakel *et al*. [5,12] used dynamic light scattering to observe the transition from Brownian to subdiffusive NP behavior in a polymer solution as the polymer concentration increased.

The transition was caused by the NPs becoming bound to the polymer chains.

NPs grafted to polymer brushes in a polymer melt provide a good model system for investigating anomalous diffusion, because it intrinsically has competing subdiffusive and hyperdiffusive behaviors. The subdiffusive behavior could be caused by the interaction between the polymer brushes and polymer matrix, whereas the hyperdiffusive behavior could be caused by anomalous dynamical properties of the matrix appearing slightly above T_g. Anomalous properties could include dynamical heterogeneity, which is associated with transient spatial fluctuations in the local dynamical behavior [13–16]. The dynamical behavior of polymer-grafted NPs in polymer melts has already been studied in various systems, such as correlated NP systems [17–20] and a dispersed NP system in PS with toluene [11]. However, our system is far simpler because (i) the NPs are dilute and the particle-particle interactions are negligible, and (ii) the matrix consists of a single-component amorphous polymer with no solvent.

II. ANOMALOUS DIFFUSION: CONTINUOUS-TIME RANDOM WALK MODEL APPROACH

Diffusive NP behaviors are often expressed as random walks in theoretical studies. In a standard random walk, the step length is fixed, and steps occur at discrete times separated by a fixed time interval. A more general continuous-time random walk (CTRW) [21,22] can be obtained by defining the step length as the step-length probability density, and the waiting time before each step as the waiting-time probability density. Consequently CTRW models have been widely used to model anomalous diffusion.

We employed a model that can express both hyperdiffusive and subdiffusive behavior proposed by Duri and Cipelletti [23] and Caronna *et al*. [10], hereafter abbreviated as DC-CTRW. In this model, the displacement of a NP during time interval t, consists of N discrete steps, and the probability of N events

*t-hoshino@cstf.kyushu-u.ac.jp
†takahara@cstf.kyushu-u.ac.jp

occurring during t follows a Poisson distribution:

$$P_t(N) = \exp(-\Gamma_0 t)(\Gamma_0 t)^N / N!, \tag{1}$$

where $1/\Gamma_0$ is the mean time between events. Using the degree of correlation $h(q,N)$, where q is the scattering vector, the intermediated scattering function $f(q,t)$, which we will relate to the time-autocorrelation function obtained by XPCS later, is expressed by

$$f(q,t) = \sum_{N=0}^{\infty} P_t(N)h(q,N). \tag{2}$$

$h(q,N)$ can be modeled and it was argued that [23,24]

$$h(q,N) = \langle \exp(-iN^\alpha \mathbf{q} \cdot \mathbf{R}) \rangle, \tag{3}$$

where the averaging is over all particles and all orientations of $\mathbf{q}$. The parameter α has a value between 0 and 1 that determines the particle behavior, and $\mathbf{R}$ is the particle displacement in a single step. The total displacement over N steps is expressed by $N^\alpha \mathbf{R}$. Brownian motion is described by $\alpha = 0.5$, whereas $\alpha > 0.5$ and $\alpha < 0.5$ describe hyperdiffusive and subdiffusive behavior, respectively. When $\alpha = 1$, the behavior is ballistic. When the particle system is isotropic, dilute, and noninteracting, the dynamical behavior is analogous to a gaslike system, where the Gaussian distribution of $\mathbf{R}$ is used and the following expression is obtained [24]:

$$h(q,N) \approx \exp[-(qN^\alpha \delta_0)^2], \tag{4}$$

where δ_0 is the average length of a single jump.

III. EXPERIMENT

We investigated the dynamics of PS-grafted silica NPs in an atactic PS matrix as the temperature was increased above the PS matrix T_g. The PS-grafted silica NPs were prepared by the grafting-from method using the surface initiator (2-bromo-2-methyl) propionyloxyhexyltriethoxysilane [25,26]. The silica NPs (110 nm diameter; Nissan Chemicals) grafted with PS brushes ($M_w = 3.24 \times 10^4$ g mol^{-1}, $M_w/M_n = 1.41$, and 0.28 chains nm^{-2}) were dispersed in the PS matrix ($M_w = 1.14 \times 10^4$ g mol^{-1}, $M_w/M_n = 1.09$). The silica concentration was adjusted to be 0.96 vol %. T_g of the PS matrix is 367 K measured by differential scanning calorimetry. The static state of the sample was investigated by ultra-small-angle x-ray scattering (USAXS) performed on the BL19B2 beamline of SPring-8 (Japan). The USAXS intensity profile can be expressed very well by the form factor of a sphere given by a Gaussian size distribution with a mean radius of 55 nm and a root mean square deviation of 4 nm, which showed the silica NPs were well dispersed in the PS matrix and did not form aggregates [27].

The XPCS measurements were performed on the BL19LXU beamline of SPring-8 with a 27-m-long undulator [28]. The undulator source and Si(111) monochromator were tuned to an energy of 8.00 keV and higher harmonic x rays were removed by Pt-coated mirrors. The transverse coherence of the incident x rays was $\xi_t \approx 16$ μm $\times$ 132 μm ($H \times V$) at the sample position. In order to make sure of transverse coherence, the beam size was reduced with slits to 20 μm $\times$ 20 μm upstream of the sample. The parasitic scattering was

shielded by the other slits and a pinhole, and the sample was irradiated with partially coherent x rays in a vacuum. The scattered x rays were detected by a two-dimensional hybrid pixel array detector (PILATUS 100 K, DECTRIS) with the grid mask resolution enhancer mounted $\sim$3.5 m downstream of the sample [29]. For the measurements, 5000–20 000 images were taken with an exposure time of 10–100 ms and a readout time of 3 ms. The XPCS measurements were conducted between 433 and 503 K using a copper cell with aluminum windows designed for eliminating the thermal gradient [30].

In the XPCS experiments, the sample was kept at the target temperature for $\sim$2 h, and then the XPCS measurements were repeated every 30 min until no further change was observed. After completing each measurement at a given temperature, the measurement was repeated at the initial temperature to confirm no x-ray-induced damage to the sample had occurred.

During the XPCS measurements, the fluctuation of the scattering intensity $I(q,t)$, at a scattering vector q, is obtained in a time series t, and the intensity time-autocorrelation function $g_2(q,t)$ is evaluated as

$$g_2(q,t) = \langle I(q,t')I(q,t'+t) \rangle / \langle I(q,t') \rangle^2, \tag{5}$$

where the angle brackets indicate time averaging.

IV. RESULTS AND DISCUSSIONS

A. Empirical fitting analysis

Figure 1 shows representative data for the measured $g_2(q,t)$. They were taken at $q = 2.15 \times 10^{-2}$ nm^{-1} at various temperatures from 443 to 503 K. At low temperatures, $g_2(q,t)$ was damped slowly, because of the high viscosity of the PS matrix. The damping rate became higher as the temperature increased owing to the decrease of the PS matrix viscosity. The relaxation rate and the shape of $g_2(q,t)$ are evaluated by fitting to an exponential function,

$$g_2(q,t) = \beta \exp[-2(\Gamma t)^\gamma] + 1, \tag{6}$$

where β is the speckle contrast, Γ is the relaxation rate, and γ is the stretched or compressed exponent. The typical value of β was $\sim$0.02 with a slight q dependence, which was
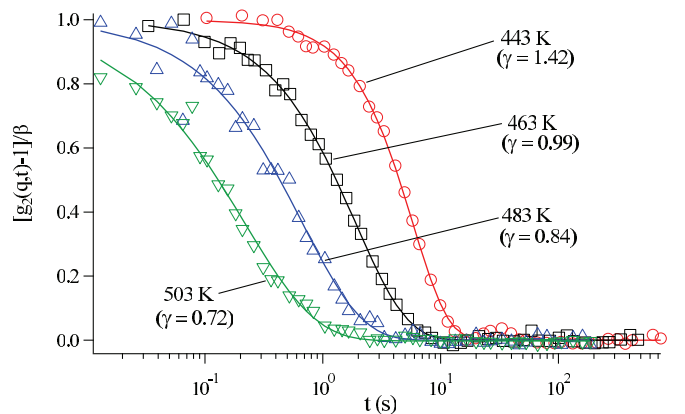
FIG. 1. (Color online) Representative results of the normalized autocorrelation functions (symbols) measured at $q = 2.15 \times 10^{-2}$ nm^{-1} for the PS-grafted nanoparticles dispersed in a PS matrix at different temperatures. Solid lines are fitting curves for Eq. (6).
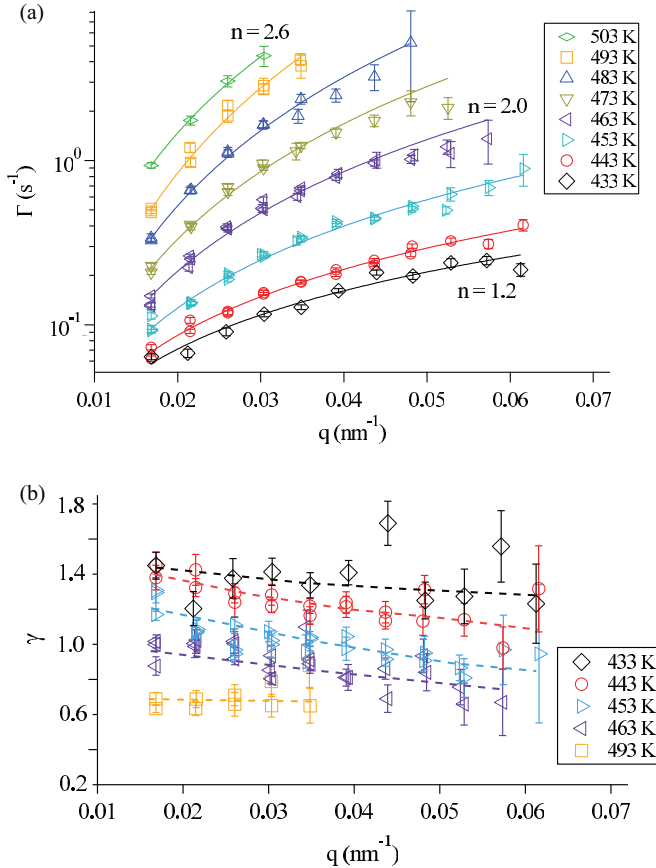
FIG. 2. (Color online) (a) q dependence of Γ obtained from the fitting results of Eq. (6). Solid lines are the $\Gamma \propto q^n$ power law fitting curves. (b) Representative q dependence of γ obtained from the fitting results of Eq. (6). For clarity, γ at 473, 483, and 503 K are not shown. The dashed lines are visual guides.

consistent with the estimated value from the speckle size and the hole size of the grid mask on the detector. Equation (6) fits the experimental $g_2(q,t)$ data well (solid lines, Fig. 1) with $\gamma = 1.43$, 0.99, 0.84, and 0.72, at $T = 443$, 463, 483, and 503 K, respectively. The values of Γ and γ obtained from the fitting analysis with Eq. (6) are plotted against q in Fig. 2. The solid lines in Fig. 2(a) are the fitting curves for Γ with power law behavior of $\Gamma \propto q^n$, and $n = 1.18$, 1.34, 1.66, 2.02, 2.34, 2.60, 2.94, and 2.64 at $T = 433$, 443, 453, 463, 473, 483, 493, and 503 K, respectively. For simple Brownian motion, $\gamma = 1$ and $\Gamma = Dq^2$, where D is the diffusion coefficient. Therefore, our results show the NP behavior was non-Brownian. Although such anomalous behavior has been often observed in nonequilibrium systems, we have not observed any time dependence in our covered time range of a few hours.

B. Fitting analysis based on the DC-CTRW model

To understand the NP behavior on a microscopic scale, the experimental data were analyzed with the DC-CTRW model. For the DC-CTRW model, $\gamma > 1$ at $q \to 0$ for hyperdiffusive NP behavior [10,23]. We examined the temperature dependence of the NP behavior quantitatively.

Using $f(q,t)$, $g_2(q,t)$ can be expressed as

$$g_2(q,t) = 1 + \beta \, |f(q,t)|^2 \,. \qquad (7)$$

Equations (2) and (7) were used to fit the experimental data, and a global fitting procedure was adopted. $g_2(q,t)$ at various q and at a given temperature were simultaneously fitted with Eqs. (2) and (7) using fitting parameters α, Γ_0, and δ_0 common to all these data sets. Some of the fitting curves obtained by the DC-CTRW model are shown in the insets of Figs. 3(a), 3(c), and 3(e), respectively. The fitting curves reproduced all the experimental data. In Fig. 3, the damping rate (Γ) and shape (γ) of $g_2(q,t)$ calculated using Eqs. (2) and (7) with $(\alpha, \delta_0, \Gamma_0) = (0.69, 8.7 \text{ nm}, 1.1 \text{ s}^{-1})$, $(0.40, 17.4 \text{ nm}, 4.7 \text{ s}^{-1})$ and $(0.35, 24.9 \text{ nm}, 11.7 \text{ s}^{-1})$ at 443, 473, and 503 K, respectively, are indicated by solid lines. Figures 3(a) and 3(b) show that the experimental values of Γ increased almost linearly and γ gradually decreased with q. The values and trend were reproduced well by the DC-CTRW model. Similar results were obtained at $T \leqslant 453$ K. However, Figs. 3(c) and 3(d) show that although the q dependence of Γ agreed well with values calculated by the DC-CTRW model at 473 K, the q dependence of γ was not perfectly reproduced, as well as Figs. 3(e) and 3(f) at 503 K. In the subdiffusion regime, γ calculated with the DC-CTRW model increased slightly with q, whereas the experimental data showed γ stayed almost constant or slightly decreased. The same trend was observed at $T > 453$ K. These differences imply that there may be a better model for representing the subdiffusive behavior of PS-grafted NPs in the PS matrix. A discussion of the subdiffusive behavior in another model is presented in the Appendix.

The values of α, δ_0, and Γ_0 obtained from the DC-CTRW analysis at each temperature are plotted against temperature in Fig. 4. Although $\alpha = 0.84$ at 433 K, it decreased as the temperature increased and dropped below 0.5 between 453 and 463 K. At $T \geqslant 463$ K, $\alpha < 0.5$, indicating that although the NP behavior is almost ballistic and hyperdiffusive at $T \leqslant 453$ K, it changed from hyperdiffusive to subdiffusive behavior between 453 and 463 K. The crossover temperature from hyperdiffusion to subdiffusion was estimated by the interpolation method as 457 K, which is $1.25T_g$. This temperature is very close to the crossover temperature of $1.26T_g$ between hyperdiffusion ($\alpha > 0.5$) and Brownian diffusion ($\alpha = 0.5$) observed in the silica NP system suspended in glass-forming liquid (propanediol) by Caronna *et al.* [10]. The hyperdiffusive behavior observed in this system at low temperatures may be associated with the dynamical heterogeneity of the surrounding matrix, because the heterogeneity may impose a preferential direction of motion.

At high temperatures in our system ($T > 1.25T_g$), α is smaller than 0.5 (subdiffusive) which means that the migration of NPs is constrained rather than simple Brownian behavior. This difference between Brownian behavior in the propanediol system and subdiffusive behavior in our PS system may be caused by differences between the liquid and polymer matrix. The subdiffusive NP behavior caused by the entanglement effect of the polymer matrix was observed in PS solutions in xylene [6], where the molecular weight of PS was much higher than the entanglement molecular weight, M_e. In our system, the molecular weight of the PS matrix ($M_w = 1.14 \times 10^4 \text{ g mol}^{-1}$) was smaller than $M_e \approx 1.8 \times 10^4 \text{ g mol}^{-1}$ [31]; thus the
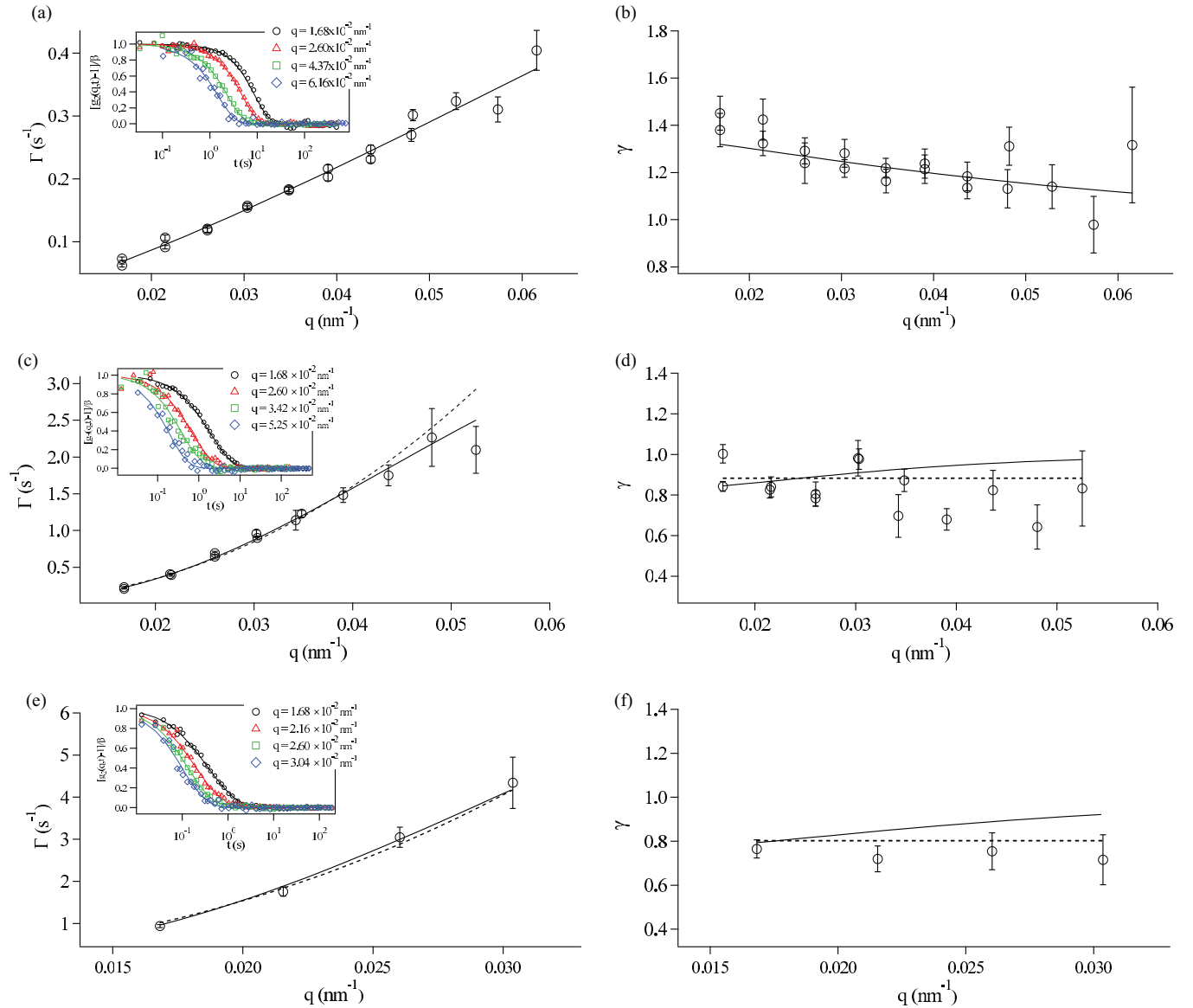
FIG. 3. (Color online) q dependence of (a) Γ and (b) γ at 443 K, of (c) Γ and (d) γ at 473 K, and of (e) Γ and (f) γ at 503 K. Representative normalized autocorrelation functions and fitting curves for Eqs. (2) and (7) at various q are shown in the insets. Solid lines are DC-CTRW model values, where $(\alpha, \delta_0, \Gamma_0) = (0.69, 8.7\text{ nm}, 1.1\text{ s}^{-1})$, $(0.4, 17.4\text{ nm}, 4.7\text{ s}^{-1})$, and $(0.35, 24.9\text{ nm}, 11.7\text{ s}^{-1})$ for 443, 473, and 503 K, respectively. Dashed lines in (c) and (d) for 473 K are sub-CTRW model values with $(\zeta, K_\zeta) = (0.90, 969\text{ nm}^2\text{ s}^{-\zeta})$ and dashed lines in (e) and (f) for 503 K are with $(0.84, 3692\text{ nm}^2\text{ s}^{-\zeta})$, which are explained in the Appendix.

polymer chains of the PS matrix should not cause subdiffusive behavior through entanglement. In contrast, the molecular weight of the grafted PS brushes ($M_\text{w} = 3.24 \times 10^4\text{ g mol}^{-1}$) was larger than M_e. The entanglement of the PS brushes and the PS matrix may cause the subdiffusive NP behavior. Moreover, it has been reported that the polymer matrix chains, which are shorter than those of the brushes, can intrude into the brushes and wet brushes because of entropic interactions [32–37]. This observed crossover between subdiffusion and hyperdiffusion may be explained as follows: The NPs are trapped in the PS matrix due to the entanglement effect between the PS brushes and the PS matrix, and they migrate with a jump to other sites via release process. In the subdiffusive regime at $T > 1.25\,T_\text{g}$, the direction of the jump may be isotropic. On the other hand,

in the hyperdiffusive regime at $T < 1.25T_\text{g}$, heterogeneity of the PS matrix may impose a preferential direction.

The average length of a single jump, δ_0, increased [Fig. 4(b)], and the mean time between events, $1/\Gamma_0$, decreased as the temperature increased [Fig. 4(c)]. This may arise from the increased thermal agitation and the decrease in the PS matrix viscosity η as the temperature increased. Figure 5 shows the temperature dependence of the effective particle velocity, $v_0 = \delta_0\Gamma_0$, which increased rapidly with temperature. To investigate the effect of temperature T and η on v_0, the scaled inverse viscosity $T\eta^{-1}$, which is $CT\eta^{-1}$, where $C = v_0\,(T = 453\text{ K})/[453\eta^{-1}(T = 453\text{ K})] = 0.73\text{ nm Pa K}^{-1}$ was calculated (dashed line in Fig. 5). The NP behavior was closest to Brownian at 453 K. Although the calculated values agreed
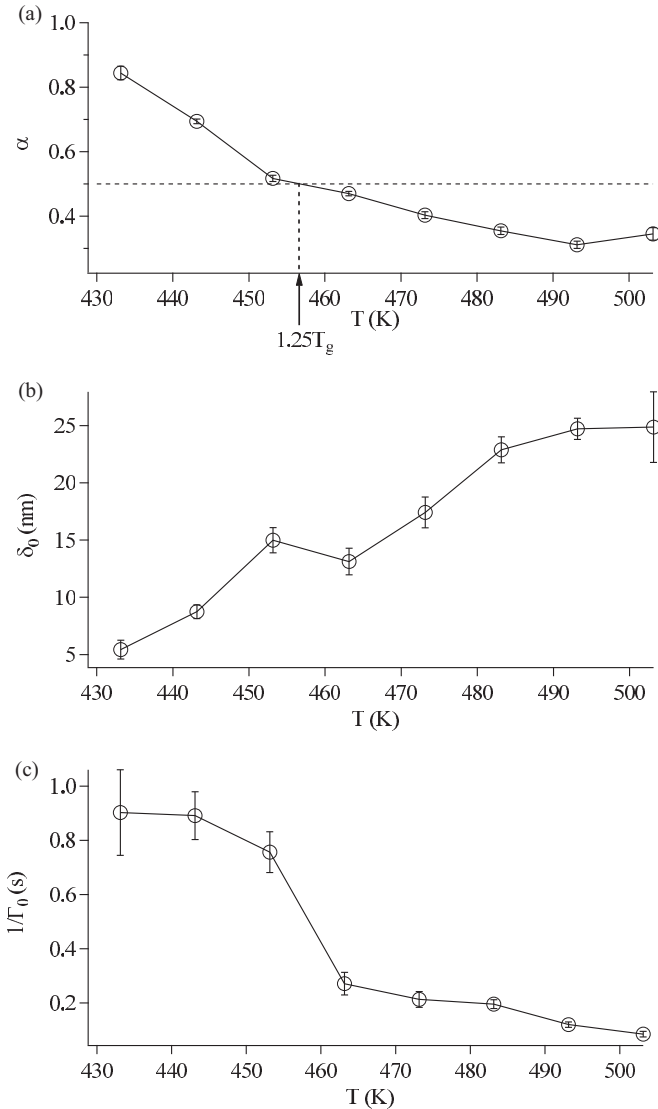
FIG. 4. Temperature dependence of fitting parameters (a) α, (b) δ_0, and (c) Γ_0 for the DC-CTRW model.
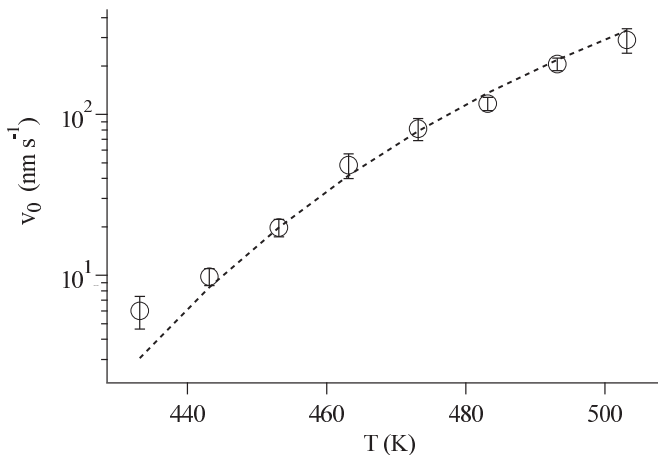
FIG. 5. Temperature dependence of $\nu_0 = \delta_0 \Gamma_0$. The dashed line is the scaled inverse viscosity, $CT\eta^{-1}$, where $C = \nu_0 (T = 453\,\mathrm{K})/[453\eta^{-1}(T = 453\,\mathrm{K})] = 0.73\,\mathrm{nm\,Pa\,K^{-1}}$.

well with the experimental temperature dependence of ν_0 in the subdiffusive regime at $463 < T < 503$ K, the calculated values were slightly larger in the hyperdiffusive regime at $T \leqslant 453$ K. This suggests that both the direction of the motion and the velocity were affected by the dynamic heterogeneity of the matrix in the hyperdiffusive regime, whereas the velocity was dominated by the viscosity of the homogeneous matrix in the subdiffusive region.

V. CONCLUSION

We investigated the dynamical behavior of PS-grafted silica NPs in a PS matrix ($T_g \approx 367$ K) at 433–503 K by using XPCS. The time-autocorrelation functions showed temperature dependent relaxation behavior and non-Brownian features. The behavior was analyzed quantitatively on a microscopic scale by using fitting analysis based on the CTRW model. The crossover from hyperdiffusion to subdiffusion was observed at $1.25T_g$. Moreover, the estimated effective NP velocity deviated from $T\eta^{-1}$ as the temperature decreased in the hyperdiffusive regime, whereas it was proportional to $T\eta^{-1}$ in the subdiffusive regime.

APPENDIX: FITTING ANALYSIS USING THE SUBDIFFUSIVE CTRW MODEL

1. CTRW model for subdiffusion

In the DC-CTRW model, the anomalous behavior is expressed by introducing α ($\neq 0.5$). While $\alpha > 0.5$ describes the ballisticlike behavior, the physical origin of $\alpha < 0.5$ in the subdiffusive regime is not really clear. We examined the suitability of another CTRW model, which is commonly used for expressing subdiffusive behavior.

The subdiffusive behavior of the PS-grafted NPs is assumed to be an adsorption process with a distribution of release time. In many CTRW models, the waiting-time probability distribution function $\psi(t)$ is used instead of $P_t(N)$. For example, the Poisson distribution in Eq. (1) can be replaced by the exponential function $\psi(t) = \lambda e^{-\lambda t}$. The subdiffusive motion composed of a hopping process between random adsorption sites can often be explained by a long-tailed waiting-time probability distribution function with asymptotic behavior

$$\psi(t) \sim A_\zeta (\tau/t)^{1+\zeta} \quad \text{for } 0 < \zeta < 1, \tag{A1}$$

which is introduced by Scher and Montroll [38] in order to express anomalous diffusion of electron hopping among random molecular sites by extending the works by Scher and Lax [39,40]. This has been widely accepted and developed for

expressing subdiffusive CTRW [21,22,41–43]. The particle displacement during a single step is defined in the same way as in the DC-CTRW model: using the Gaussian distribution and with an average of δ_0. In this case, the three-dimensional probability distribution function at position **r** at time t is [44]

$$W(\mathbf{r},t) = \frac{1}{4\pi K_\zeta t^\zeta r^2} \sum_{n=0}^{\infty} \frac{(-1)^n}{n!\,\Gamma[1-\zeta(1+n/2)]} \left(\frac{r^2}{K_\zeta t^\zeta}\right)^{n/2},$$
(A2)

where $K_\zeta = \delta_0^2/t^\zeta$ represents the generalized diffusion coefficient. If the particle system is isotropic, the intermediate scattering function can be written as [24]

$$f(q,t) = \int W(\mathbf{r},t)\exp(i\mathbf{q}\cdot\mathbf{r})d\mathbf{r}$$

$$= \int_0^\infty 4\pi r^2 W(\mathbf{r},t)\frac{\sin(qr)}{qr}dr. \quad \text{(A3)}$$

Hereafter this CTRW model will be referred to as the sub-CTRW model.

2. Fitting analysis based on the sub-CTRW model

Although the fitting using the DC-CTRW model showed good agreement with the experimental data, the q dependence of γ did not agree in the subdiffusive regime [Figs. 3(c)–3(f)]. In the analysis based on the sub-CTRW model, a global fitting procedure was also adopted. The experimental $g_2(q,t)$ at various values of q at a given temperature were simultaneously fitted with Eqs. (A3) and (7), with fitting parameters ζ and K_ζ common to all these data sets. Figures 3(c)–3(f) show representative calculations of Γ and γ for $g_2(q,t)$ using the sub-CTRW model, obtained at 473 and 503 K with $(\zeta, K_\zeta) = (0.90, 969\text{ nm}^2\text{ s}^{-\zeta})$ and $(0.84, 3692\text{ nm}^2\text{ s}^{-\zeta})$ shown as dashed lines. Γ and γ calculated with the sub-CTRW model agree well with the experimental values. In particular, γ was constant when it was plotted as a function of q, unlike the values calculated with the DC-CTRW model, which increased with q. Similar trends were also observed at $T \geqslant 463$ K. Hence, the sub-CTRW model may be more appropriate than the DC-CTRW model for expressing the dependence of q on γ in the subdiffusive regime.

[1] I. Golding and E. C. Cox, Phys. Rev. Lett. **96**, 098102 (2006).

[2] G. Guigas, C. Kalla, and M. Weiss, Biophys. J. **93**, 316 (2007).

[3] I. Y. Wong, M. L. Gardel, D. R. Reichman, E. R. Weeks, M. T. Valentine, A. R. Bausch, and D. A. Weitz, Phys. Rev. Lett. **92**, 178101 (2004).

[4] R. A. Omari, A. M. Aneese, C. A. Grabowski, and A. Mukhopadhyay, J. Phys. Chem. B **113**, 8449 (2009).

[5] J. Sprakel, J. van der Gucht, M. A. Cohen Stuart, and N. A. M. Besseling, Phys. Rev. Lett. **99**, 208301 (2007).

[6] H. Guo, G. Bourret, R. B. Lennox, M. Sutton, J. L. Harden, and R. L. Leheny, Phys. Rev. Lett. **109**, 055901 (2012).

[7] L. Cipelletti, S. Manley, R. C. Ball, and D. A. Weitz, Phys. Rev. Lett. **84**, 2275 (2000).

[8] B. Chung, S. Ramakrishnan, R. Bandyopadhyay, D. Liang, C. F. Zukoski, J. L. Harden, and R. L. Leheny, Phys. Rev. Lett. **96**, 228301 (2006).

[9] M. Bellour, A. Knaebel, J. L. Harden, F. Lequeux, and J. P. Munch, Phys. Rev. E **67**, 031405 (2003).

[10] C. Caronna, Y. Chushkin, A. Madsen, and A. Cupane, Phys. Rev. Lett. **100**, 055702 (2008).

[11] H. Guo, G. Bourret, M. K. Corbierre, S. Rucareanu, R. B. Lennox, K. Laaziri, L. Piche, M. Sutton, J. L. Harden, and R. L. Leheny, Phys. Rev. Lett. **102**, 075702 (2009).

[12] J. Sprakel, J. van der Gucht, M. A. Cohen Stuart, and N. A. M. Besseling, Phys. Rev. E **77**, 061502 (2008).

[13] C. Angell, J. Phys. Chem. Solids **49**, 863 (1988).

[14] S. Sastry, P. Debenedetti, and F. Stillinger, Nature **393**, 554 (1998).

[15] M. Ediger, Annu. Rev. Phys. Chem. **51**, 99 (2000).

[16] P. Debenedetti and F. Stillinger, Nature **410**, 259 (2001).

[17] A. K. Kandar, S. Srivastava, J. K. Basu, M. K. Mukhopadhyay, S. Seifert, and S. Narayanan, J. Chem. Phys. **130**, 121102 (2009).

[18] S. Srivastava, S. Chandran, A. K. Kandar, C. K. Sarika, J. K. Basu, S. Narayanan, and A. Sandy, J. Chem. Phys. **133**, 151105 (2010).

[19] S. Chandran, C. K. Sarika, A. K. Kandar, J. K. Basu, S. Narayanan, and A. Sandy, J. Chem. Phys. **135**, 134901 (2011).

[20] P. Akcora, S. K. Kumar, J. Moll, S. Lewis, L. S. Schadler, Y. Li, B. C. Benicewicz, A. Sandy, S. Narayanan, J. Illavsky, P. Thiyagarajan, R. H. Colby, and J. F. Douglas, Macromolecules **43**, 1003 (2010).

[21] J. P. Bouchaud and A. Georges, Phys. Rep. **195**, 127 (1990).

[22] R. Metzler and J. Klafter, Phys. Rep. **339**, 1 (2000).

[23] A. Duri and L. Cipelletti, Europhys. Lett. **76**, 972 (2006).

[24] B. J. Berne and R. Pecora, *Dynamic Light Scattering* (Wiley, New York, 1976).

[25] K. Ohno, T. Morinaga, K. Koh, Y. Tsujii, and T. Fukuda, Macromolecules **38**, 2137 (2005).

[26] M. Kobayashi and A. Takahara, Chem. Lett. **34**, 1582 (2005).

[27] Figure 2(b) in T. Hoshino, D. Murakami, K. Ito, Y. Tanaka, S. Sasaki, M. Takata, H. Jinnai, and A. Takahara, Polym. J. **45**, 94 (2013).

[28] M. Yabashi, T. Mochizuki, H. Yamazaki, S. Goto, H. Ohashi, K. Takeshita, T. Ohata, T. Matsushita, K. Tamasaku, Y. Tanaka, and T. Ishikawa, Nucl. Instrum. Methods Phys. Res., Sect. A **467**, 678 (2001).

[29] T. Hoshino, M. Kikuchi, D. Murakami, Y. Harada, K. Mitamura, K. Ito, Y. Tanaka, S. Sasaki, M. Takata, H. Jinnai, and A. Takahara, J. Synchrotron Radiat. **19**, 988 (2012).

[30] T. Hoshino, D. Murakami, K. Ito, Y. Tanaka, S. Sasaki, M. Takata, H. Jinnai, and A. Takahara, Polym. J. **45**, 94 (2013).

[31] L. J. Fetters, D. J. Lohse, S. T. Milner, and W. W. Graessley, Macromolecules **32**, 6847 (1999).

[32] R. Jones, L. Norton, K. Shull, E. Kramer, G. Felcher, A. Karim, and L. Fetters, Macromolecules **25**, 2359 (1992).

[33] M. Aubouy, G. Fredrickson, P. Pincus, and E. Raphael, Macromolecules **28**, 2979 (1995).

[34] C. Clarke, R. Jones, J. Edwards, K. Shull, and J. Penfold, Macromolecules **28**, 2042 (1995).

[35] G. Grest, J. Chem. Phys. **105**, 5532 (1996).

[36] G. Reiter, P. Auroy, and L. Auvray, Macromolecules **29**, 2150 (1996).

[37] P. Ferreira, A. Ajdari, and L. Leibler, Macromolecules **31**, 3994 (1998).

[38] H. Scher and E. W. Montroll, Phys. Rev. B **12**, 2455 (1975).

[39] H. Scher and M. Lax, Phys. Rev. B **7**, 4491 (1973).

[40] H. Scher and M. Lax, Phys. Rev. B **7**, 4502 (1973).

[41] H. Scher, M. Shlesinger, and J. Bendler, Phys. Today **44** (1), 26 (1991).

[42] I. M. Sokolov and J. Klafter, Phys. Rev. Lett. **97**, 140602 (2006).

[43] Y. He, S. Burov, R. Metzler, and E. Barkai, Phys. Rev. Lett. **101**, 058101 (2008).

[44] E. Barkai, Phys. Rev. E **63**, 046118 (2001).